Decorrelation of Troposphere Across Short Baselines

David Lawrence, *Novariant Corporation*,
Richard B. Langley, Donghyun Kim, *University of New Brunswick*
Fang-Cheng Chan, Boris Pervan, *Illinois Institute of Technology*

Abstract - *The performance of GNSS RTK systems is strongly dependent on spatial correlation of tropospheric errors. However, normal storm activity can cause conditions where tropospheric delays can be significantly different even across relatively short baselines. In this paper, the decorrelation of tropospheric delay over short baselines (2 to 10 km) is investigated. Data from pairs of CORS stations as well as independently collected data are used to derive double-difference phase residuals for L1 and L2 measurements. The known coordinates of the ends of the baseline are accounted for in the calculation of the residuals to provide a measurement of double-difference phase errors. Multipath contributions to the phase errors are minimized by comparing data collected on consecutive days. Tropospheric effects are isolated from ionospheric effects by looking for signatures unique to the troposphere. One such signature is the relative magnitude of the L1 and L2 residuals. A second signature is correlation with local weather data and absence of correlation with ionospheric activity. A strong correlation is seen between storm activity shown on local weather radar and high residuals. Residuals attributed to the troposphere equivalent to at least 12 parts per million for overhead satellites are observed across short baselines.*

I. INTRODUCTION

Global navigation satellite system (GNSS) real-time kinematic (RTK) systems typically rely on differential carrier phase errors being a small fraction of a carrier cycle both when searching for integers and when calculating position fixes with known integers. Under fair multipath and atmospheric conditions, and over baselines shorter than a few tens of kilometers, medium to high elevation angle satellites usually experience differential carrier phase errors significantly smaller than 0.25 cycles. However, multipath, ionosphere, and troposphere all have the potential to induce larger phase errors. Carrier phase multipath is independent of baseline length and can be reduced by proper choice of antenna and occupation site when possible. Atmospheric errors for a differential GNSS system worsen with baseline length due to spatial decorrelation of the atmospheric delays. Global models such as [1] and [2] for troposphere and [3] and [4] for ionosphere can remove the large-scale error trends from the measurements. Dual frequency processing can be used to almost completely eliminate residual ionosphere errors in an RTK system. On the other hand, little can be done about residual troposphere errors in a traditional RTK system because they affect all frequencies identically. In fact, when tracking only four satellites in a dynamic GNSS RTK system, changes in troposphere errors are absolutely indistinguishable from a change in position. Additional satellites are needed to even detect that large phase errors might exist. Even then, only a few techniques are available for reducing the impact of residual troposphere while maintaining system availability:

- weighting satellites as a function of their elevation angle
- solving for a residual zenith delay (assumes the residual error is well modeled by a residual zenith delay times a mapping function of elevation)
- attempting to fit a surface that is a function of the azimuth and elevation of the satellite to the observed measurements (this requires several redundant satellites depending on the order of the surface)
- using networks to observe tropospheric gradients (but only if the base stations are sufficiently dense to sample the errors at the spatial equivalent of the Nyquist rate)

Depending on the nature of the tropospheric decorrelation, these techniques may or may not be successful. Fortunately, most of the time residual troposphere errors can be neglected over short RTK baselines.

II. MOTIVATION

On occasion we receive reports of slow RTK integer acquisition and frequent loss of confidence in the integer solutions. Typically, such problems only occur in bad multipath environments or across longer baselines. However, sometimes we see these RTK performance problems over baselines as short a 1 km in benign multipath environments. Attempts to correlate these

reports with ionospheric storms were unsuccessful and field data replays were not improved by ionosphere-free processing. We deployed receivers from different vendors and experienced similar results. Having excluded multipath, ionosphere, and vendor-specific RTK problems, troposphere seemed to be the only remaining explanation. There was some support for this explanation based on field reports at the time of the problems. In one test, a runway survey at Patuxent River, MD, RTK problems were experienced on a clear runway using choke-ring antennas across a baseline shorter than 1 km. The surveyor reported torrential rain at the time. In many other cases, there were reports of nearby storm activity. Most of the literature we could find dealing with troposphere decorrelation focused on longer baselines. For example, [5] shows plots of wet troposphere delay versus elevation angle for baselines of 100 km, 250 km, and 500 km.

III. BACKGROUND

A few papers did seem potentially relevant to the RTK problems we were experiencing. Skidmore and Van Graas [6] recognized that horizontal tropospheric variations due to weather fronts could adversely affect high precision aviation applications such as the Local Area Augmentation System (LAAS). Nominally LAAS accounts only for tropospheric variations due to the altitude difference between the aircraft user and reference station.

Previous reports indicate that heavy rain can contribute to tropospheric delays in addition to those attributed to water vapor. Propagation through 1 km of heavy rain can induce 1.5 cm delay at L1 [7].

Researchers have shown that the passage of weather fronts can cause anomalous effects on GPS observations. For example, [8] and [9] show that fronts can cause zenith delay changes in excess of 3.4 cm. This becomes more than 10 cm in slant delay at an elevation angle of 20°. Reference [10] indicates similar results and suggests that large gradients are attributed to humidity discontinuity around the fronts. Most previous research did not investigate the effect of troposphere decorrelation over short baselines.

IV. METHODOLOGY

To quantify the error introduced by troposphere decorrelation in a local area differential system, an error metric can be derived from the carrier phase measurement equation (1).

$$\phi_k^i \lambda_k = \Delta r^i + \tau_k + N_k^i \lambda_k + T^i - I^i \lambda_k{}^2 + M_k^i + W_k^i \qquad (1)$$

where:

k is a frequency (L1 or L2)

ϕ_k^i is the single-difference carrier-phase measurement for satellite i on frequency k (in units of cycles).

λ_k is the wavelength of frequency k.

Δr^i is the differential distance to satellite i.

τ_k is the differential clock error plus other satellite-independent effects such as differential line bias on frequency k.

N_k^i is a differential cycle ambiguity[1] for satellite i and frequency k.

T^i is the differential troposphere delay for satellite i.

$I^i \lambda_k{}^2$ is the differential ionosphere group delay at frequency k.

M_k^i is the differential carrier multipath error for satellite i and frequency k.

W_k^i is the differential receiver noise error for satellite i and frequency k.

Given accurate (cm or better) knowledge of the relative positions of the antennas and resolved cycle ambiguities, these known quantities can be subtracted from the measured carrier phase to yield:

$$\Phi_k^i = \frac{\tau_k'}{\lambda_k} + \frac{T^i}{\lambda_k} - I^i \lambda_k + \frac{M_k^i + W_k^i}{\lambda_k} \qquad (2)$$

where:

τ_k' is τ_k plus the integer cycle ambiguity for a reference satellite.

$$\Phi_k^i = \phi_k^i - \frac{\Delta r^i}{\lambda_k} - N_k'^i$$

$N_k'^i$ is the double-difference cycle ambiguity for satellite i and frequency k relative to the reference satellite.

[1] Note that throughout most of this paper, the cycle ambiguities that minimize the residual errors are used. For cases when the phase errors exceed half of a cycle, these cycle ambiguities are not necessarily the correct ambiguities.

One metric for assessing the combined effect of all of the error sources is a double-difference phase residual for two satellites.

$$R_k^{mn} = \Phi_k^m - \Phi_k^n \tag{3}$$

$$R_k^{mn} = \frac{T^m - T^n}{\lambda_k} - (I^m - I^n)\lambda_k + \frac{M_k^{mn} + W_k^{mn}}{\lambda_k} \tag{4}$$

where:

R_k^{mn} is the double-difference phase residual between satellites m and n.

$$M_k^{mn} = M_k^m - M_k^n$$
$$W_k^{mn} = W_k^m - W_k^n$$

Specifically, (4) can be written as (5) and (6) for the L1 and L2 frequencies respectively:

$$R_1^{mn} = \frac{T^m - T^n}{\lambda_1} - (I^m - I^n)\lambda_1 + \frac{M_1^{mn} + W_1^{mn}}{\lambda_1} \tag{5}$$

$$R_2^{mn} = \frac{T^m - T^n}{\lambda_2} - (I^m - I^n)\lambda_2 + \frac{M_2^{mn} + W_2^{mn}}{\lambda_2} \tag{6}$$

Note that there is a fixed ratio between the contribution of the troposphere to the R_2^{mn} and R_1^{mn} residuals. Similarly, there is a fixed ratio between the contribution of the ionosphere to the R_2^{mn} and R_1^{mn} residuals. Specifically, on a plot with R_2^{mn} on the vertical axis and R_1^{mn} on the horizontal axis, the troposphere contribution is a vector with a slope of λ_1 / λ_2 and the ionosphere contribution is a vector with a slope of λ_2 / λ_1. The multipath and noise error terms have no such fixed relationship. Although there may arguably be some correlation between L1 and L2 multipath errors, a long-term scatter plot of the multipath contribution to the residuals would typically show an effectively uncorrelated error distribution (typically a circular cloud of points).

In some cases, it is desirable to have a metric similar to the double-difference residual that is specific to a single satellite rather than a pair of satellites. For example, such a metric enables a plot of error versus elevation angle. To generate such a metric, $\hat{\tau}_k$ can be estimated as the average of $\Phi_k^i \lambda_k$ across some or all satellites in view. When this estimate of the differential clock error is subtracted from each individual $\Phi_k^i \lambda_k$, it yields a double difference residual where a composite error is subtracted from one satellite's error instead of choosing a specific second satellite to eliminate the clock term. Although it is tempting to treat this residual as a function only of the differential phase errors on the individual satellite, one must recognize that it is still a double difference. The composite error may sometimes be disproportionately affected by one satellite with a large phase error or a few satellites with phase errors of the same sign. However, in many cases the composite error will be small and it is a useful approximation to neglect it. In this paper, this composite double-difference residual will be used in plots of residual versus elevation angle.

Although only double-difference error metrics are available due to clock uncertainty, a goal of this paper is to bound the single-difference phase error. One way to find a bound on the single-difference phase error is to find the clock solution that minimizes the maximum satellite residual. That is, if we define the maximum satellite error as a function of an assumed clock error:

$$E_{\max}(\hat{\tau}_k) \equiv \max_{i=1,\ldots,S} \left(\left| \Phi_k^i \lambda_k - \hat{\tau}_k \right| \right)$$

where:

S is the number of satellites,

then we know that the error on some satellite is greater than or equal to the minimum of $E_{\max}(\hat{\tau}_k)$ over all $\hat{\tau}_k$:

$$E_{bound} \equiv \min_{\hat{\tau}_k} \left(E_{\max}(\hat{\tau}_k) \right)$$

This approach neglects the impact of the elevation angle on the phase error. Therefore, if we find a large minimum bound, it may be discounted as resulting from a large phase error on a low elevation angle satellite (for which we expect larger errors). A similar approach is to find the clock solution that minimizes a maximum weighted satellite residual where the weighting is a tropospheric obliquity factor (mapping function).

$$Z_{\max}(\hat{\tau}_k) \equiv \max_{i=1,\ldots,S} \frac{\left| \Phi_k^i \lambda_k - \hat{\tau}_k \right|}{\Omega_i}$$

where:

Ω_i is an obliquity factor that is a function of the elevation angle of satellite i.

$$Z_{bound} \equiv \min_{\hat{\tau}_k} \left(Z_{\max}(\hat{\tau}_k) \right)$$

The resulting minimum weighed residual, Z_{bound}, is a lower bound on the single-difference phase error projected to vertical. This minimum bound will be referred to as the zenith error bound in this paper. Presumably, the single-difference phase error for an overhead satellite can be at least as big as this bound under the atmospheric conditions of the test. Similarly, it is assumed that the phase error for a lower elevation angle satellite could be at least as big as this bound times the tropospheric obliquity factor corresponding to the lower elevation angle.

V. EXPERIMENTS

Data from the five baselines listed in Table I were analyzed for this paper. Baselines 1, 4, and 5 had CORS sites for both ends of the baseline. Baselines 2 and 3 were set up in southern Texas after reports of RTK problems. Baseline 2 had an AeroAntenna L1/L2 ARINC-style antenna on a 380 mm diameter ground plane at one occupation site and four AeroAntenna "sunflower" antennas (part number AT2775-270S) connected to a Novariant 7D Quad receiver at the other site (see Fig. 1). A Trimble MS750 was also connected to one of the four sunflower antennas. Baseline 3 shared an occupation site (the one with 4 antennas) with baseline 2. The other occupation site for the third baseline also consisted of 4 sunflower antennas connected to a Novariant 7D Quad receiver. One of the sunflower antennas was also connected to a NovAtel OEM4 receiver.

TABLE I
EXPERIMENTAL BASELINE DESCRIPTIONS

Baseline #	Baseline Length	Location
1	2128.43 m	Stennis CORS (MSSC/NDBC)
2	2857.24 m	South Texas
3	7870.67 m	South Texas
4	2659.26 m	San Marcos CORS (TXSM/CSM1)
5	5425.30 m	Seattle CORS (SEAT/SEAW)

Fig. 1. Occupation Site for Baselines 2 and 3

VI. RESULTS

On August 21, 2005, high residuals were observed on baseline 1. Fig. 2 shows the corresponding L1 residuals versus time (the different colors represent different elevation-angle-sorted channels). Note the period of higher residuals between 21:30 and 23:30. Fig. 3 shows the same data plotted versus elevation angle. Subsequent inspection of radar data from the National Climatic Data Center (NCDC) showed a storm passing through the Stennis Space Center, MS, area at the time of the high residuals. Fig. 4 shows radar data from that region at the time of the highest residuals. The two white circles represent the location of the Stennis CORS stations. One can see that the CORS stations were surrounded by moderately severe storm activity at the time.

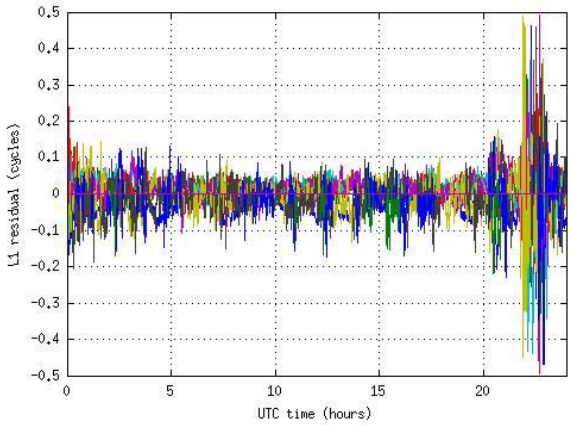

Fig. 2. Baseline 1 Residuals vs. time on 2005-08-21

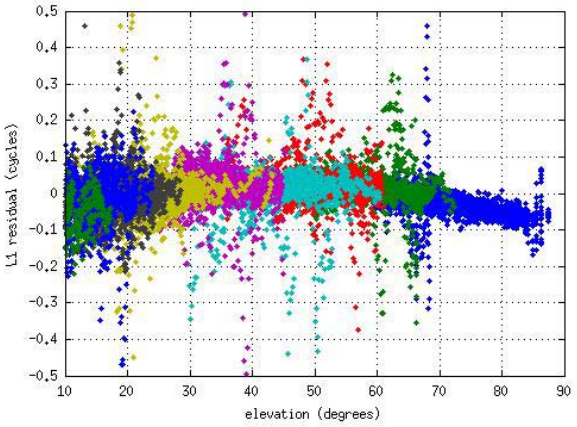

Fig. 3. Baseline 1 Residuals vs elevation on 2005-08-21

During the occupation of the sites making up baselines 2 and 3, a storm system passed through Texas. In the afternoon (CDT) of October 11th, 2005, large residuals were seen on both of those baselines. Fig. 5 shows a radar snapshot around the time of peak residual errors. The three white circles represent the location of the three occupation sites.

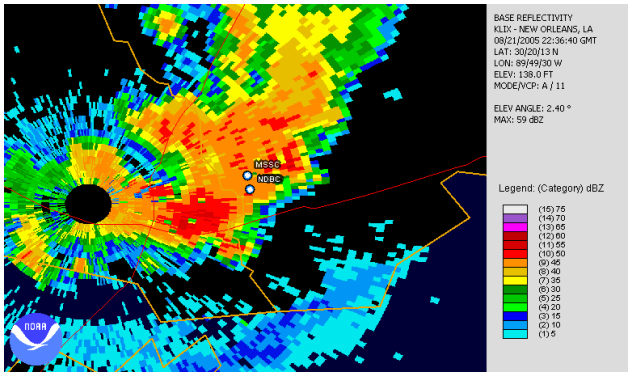

Fig. 4. Radar Data for Baseline 1 on 2005-08-21

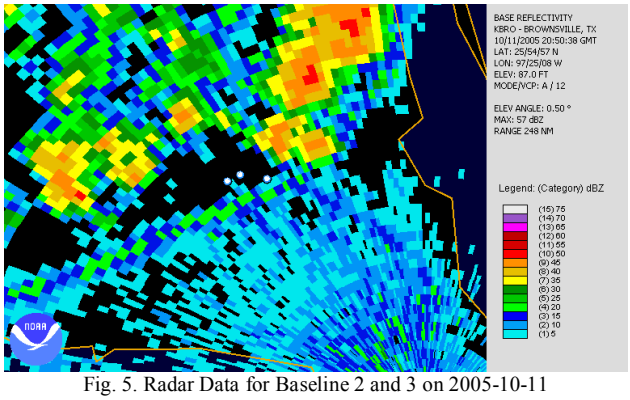

Fig. 5. Radar Data for Baseline 2 and 3 on 2005-10-11

Fig. 6 shows the L1 residuals versus time for baseline 2. The highest residuals occurred at approximately 21:00 UTC which correlated well with the time of the peak local storm activity on the weather radar. Fig. 7 shows the zenith error bound versus time for baseline 2. This bound has a maximum of 0.23 cycles. Although some of this error may be attributable to multipath, it is believed that the majority of this error resulted from the troposphere. It was determined that the maximum zenith error bound resulted from a double-difference phase error for PRN 8 and 27 of about 0.5 cycles at a time when both satellites had a high elevation angle. The clock solution that minimized the maximum error attributed roughly half of the 0.5 cycles to each of PRN 8 and PRN 27. Fig. 8 shows the double-difference error for PRN 8 and 27 for the day of the storm and the following day. The difference between the residuals on the two days is attributed to the storm (the remainder is assumed to be multipath). Correcting the maximum zenith error bound for the multipath contribution results in a bound of 0.18 cycles. This magnitude of zenith error over such a short baseline represents 12.3 parts per million of zenith troposphere decorrelation!

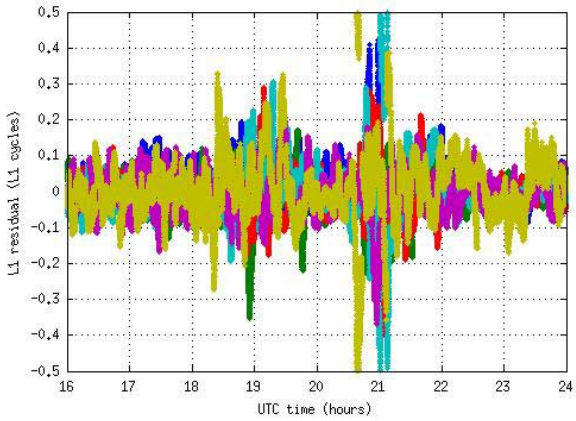

Fig. 6. Baseline 2 L1 Residual on 2005-10-11

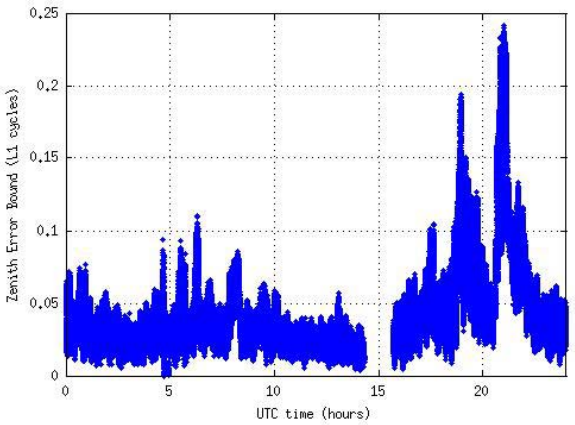

Fig. 7. Baseline 2 Zenith Error Bound on 2005-10-11

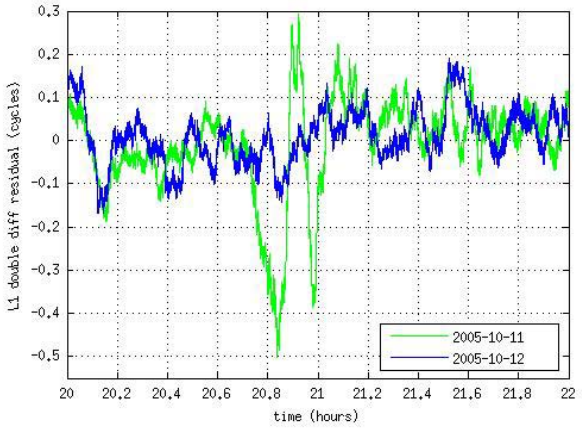

Fig. 8. Baseline 2 Double-difference Error (PRNs 8 and 27)

Fig. 9 shows the double-difference L2 versus L1 residuals for PRNs 8 and 19. Note the signature of the error clearly follows the troposphere characteristic line and not the ionosphere characteristic line. (It should be noted that some other error sources would have the same signature as troposphere, such as motion of an assumed static baseline or satellite ephemeris errors. However, we are certain that the baseline didn't move, and any ephemeris errors would have to be extremely large to result in such large errors over such a short baseline.) Another interesting plot is shown in Fig. 10, which shows the double-difference L2 versus L1 residual for PRNs 26 and 29. These two satellites were less than 18 degrees apart when viewed from southern Texas. Despite their proximity to one another, a large troposphere error signature is clear in the plot.

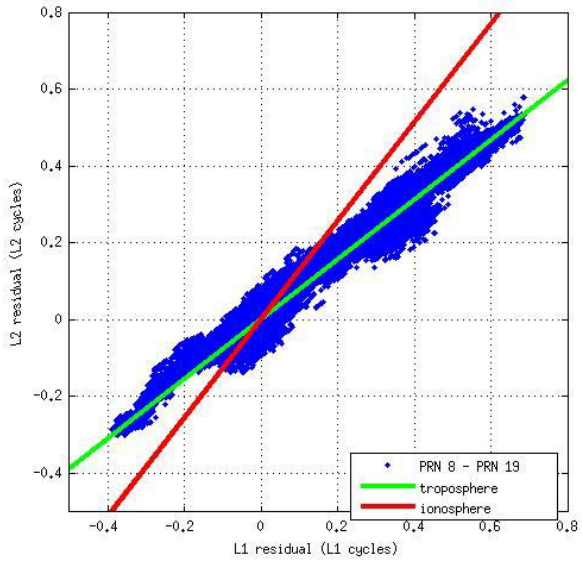

Fig. 9. Baseline 2 Double-difference Error (PRNs 8 and 19)

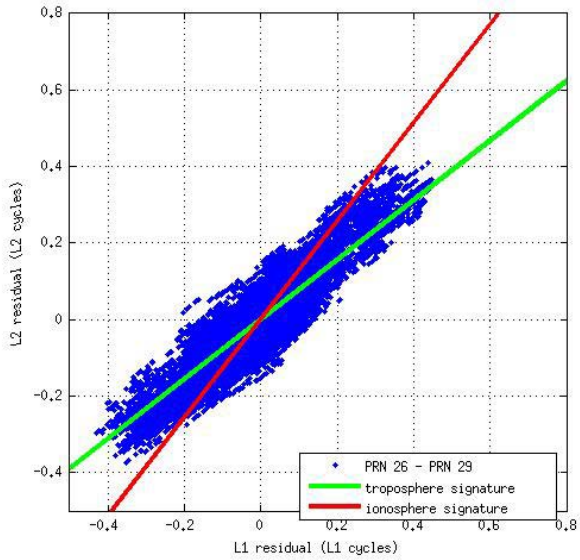

Fig. 10. Baseline 2 Double-difference Error (PRNs 26 and 29)

Fig. 11 shows the same double difference as Fig. 8 (PRNs 8 and 27) for baselines 2 and 3 on October 11th. Interestingly, although baseline 3 is almost 2.8 times as long as baseline 2, the double-difference phase error is about the same for both. Although not statistically significant, this may indicate that the decorrelation rate is fastest over the first few kilometers.

Earlier on 11th, the same storm system passed through San Marcos Texas. Fig. 12 shows a plot of double-difference L2 residual versus L1 residual for San Marcos. The double difference is between the highest elevation satellite and the third highest elevation satellite. The dark blue dots are from October 11th. The yellow dots are from another day without a storm. Note that the magnitude of the residuals is much bigger on the storm day and that the residual signature follows the characteristic line for troposphere. Although not shown in this paper, CORS data from nearby San Antonio also showed high residuals at this time.

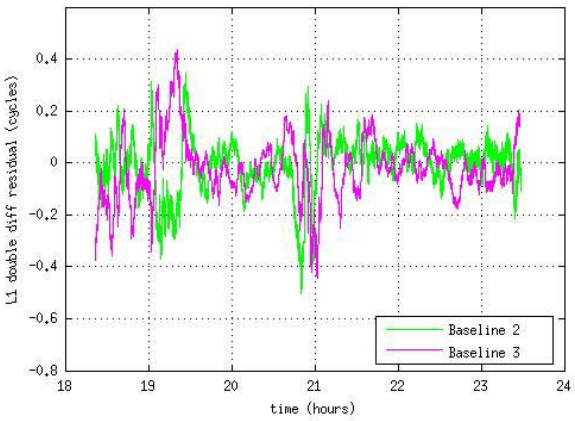

Fig. 11. Residuals for Baselines 2 and 3 on 2005-10-11

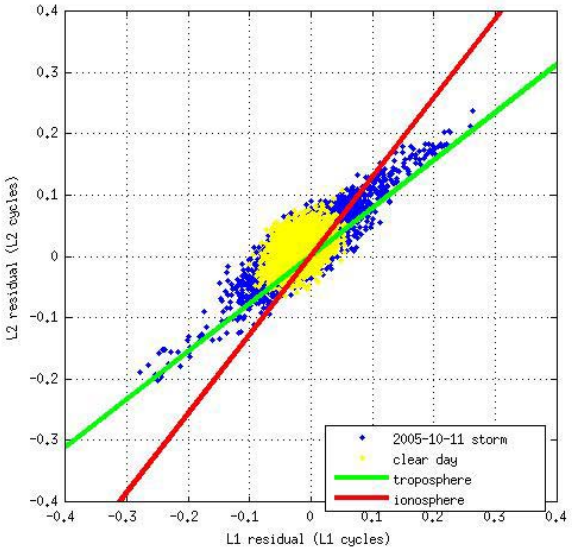

Fig. 12. Baseline 4 Residuals on 2005-10-11

On October 31st of 2005, another storm system passed through Texas. CORS station data from San Marcos were analyzed at this time and again showed evidence of troposphere-induced residual errors. Fig. 13 shows the same plot as Fig. 12, but for October 31st.

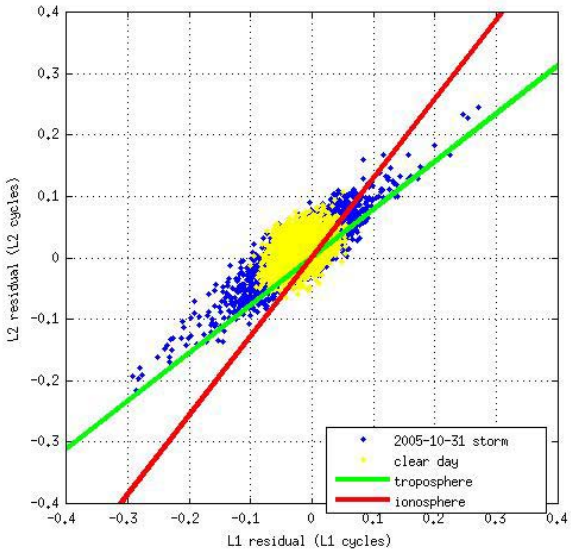

Fig. 13. Baseline 4 Residuals on 2005-10-31

To contrast against the previous results, Fig. 14 shows a plot of double-difference phase residual between PRN 20 and 25 for baseline 5 on July 15th and 16th of 2000 (soon after the so-called Bastille Day Solar Event). The plot clearly shows the signature of an ionosphere event. Note how the scatter plot closely follows the red characteristic line of the ionosphere rather than the green characteristic line of the troposphere. The double difference phase error for this pair of satellites was a maximum of 0.98 cycles on L1, or 34 parts per million (p.p.m.).

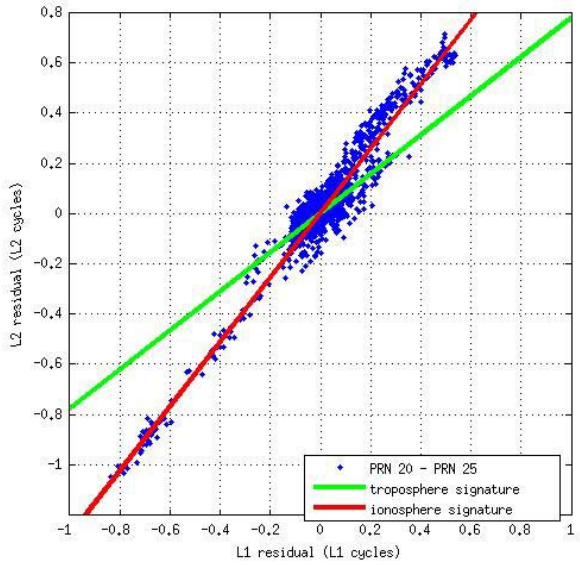

Fig. 14. Baseline 5 Residuals after Solar Event

Again to contrast with the earlier results that show the signature of troposphere, Fig. 15 shows the L1 composite

residual for the highest elevation satellite during seven relatively quiet days on baseline 1. Each color in the plot represents a different day. Note the high correlation in the error between days. This correlation is consistent with the signature of multipath. (Multipath is highly correlated on static baselines from day to day, because each GPS satellite's position in the sky repeats every sidereal day.)

The authors also analyzed data from Albuquerque, Salt Lake City, Prudoe Bay, Dover, and Raleigh Durham CORS stations. As one might expect, the first three regions showed smaller and less frequent phase error excursions relative to regions that experience frequent severe storm activity such as Texas.

VII. CONCLUSIONS

Tropospheric delay can decorrelate rapidly with distance over short baselines. Zenith decorrelation of at least 12 parts per million was observed over a 3 km baseline. No apparent spatial gradients were detected (although they cannot be ruled out). Under such conditions, RTK systems with conservative thresholds will be slow to acquire and will lose fixed integer confidence frequently. RTK systems with more aggressive thresholds designed to quickly acquire integers will frequently resolve integers incorrectly. Even if an RTK system finds the correct integers, position errors of 10 to 20 PPM are possible. Although not typical, such errors can happen with high frequency in certain regions.

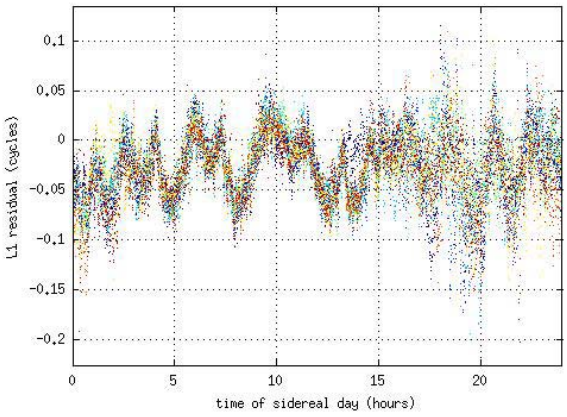

Fig. 15. Baseline 1 Multipath Data

VIII. FUTURE WORK

Future work should include both theoretical and additional experimental analysis. On the theoretical side, the physics behind this phenomenon is not well understood. Although a strong correlation between high residuals and rain shown on weather radar has been observed, it is very likely that the rain is just another effect of the storm system rather than the cause of the high residuals. A model that predicts this phenomenon should be developed (or applied specifically to short baseline RTK applications if an appropriate model already exists). On the experimental side, more data should be collected to observe the spatial decorrelation of the tropospheric delays with higher resolution. An interesting experiment would be to arrange a series of GPS receivers along a straight road at relatively close (e.g. 500 meter) periodic distances along the road and collect data from all receivers during a severe storm. An FFT could be performed on the resulting residuals to get a sense of the spatial frequency content of the troposphere error during a storm. Gradients that were not apparent on a single relatively long baseline may be more apparent in such an experiment. Note that with the future availability of two high elevation angle WAAS satellites with a fixed position in the sky, double differencing these satellites will be convenient for such tests (although the lack of an L2 carrier will prohibit plots of L1 versus L2 residuals).

ACKNOWLEDGMENTS

The authors wish to thank the following contributors. Radar data were downloaded from the NCDC. RINEX data from National and Cooperative CORS stations were invaluable in establishing a correlation between baseline residual errors and storm activity. Dennis Connor at Novariant conducted the experiments in southern Texas.

REFERENCES

[1] Collins, P. and Langley, R.B., "Tropospheric Delay: Prediction for the WAAS User," *GPS World*, Vol. 10, No. 7, 1999, pp. 52-58.

[2] Leandro, R., Santos, M., and Langley, R.B., "UNB Neutral Atmosphere Models: Development and Performance," *Proceedings of The Institute of Navigation National Technical Meeting 2006*, 18-20 January 2006, Montery, CA, pp. 564-573. .

[3] Klobuchar, J.A., "Ionospheric Time-Delay Algorithm for Single-Frequency GPS Users," *IEEE Transactions on Aerospace and Electronic Systems*, Vol. AES-23, No. 3, 1987, pp. 325-331.

[4] Hernández-Pajares, M., "IGS Ionosphere WG Status Report: Performance of IGS Ionosphere TEC Maps," *Celebrating a Decade of the International GPS Service*, Proceedings of IGS Workshop and Symposium 2004, 1-5 March 2004, Berne, Switzerland, pp. 225-250.

[5] Skone, S., "Propagation Environmental Effects on GPS," *ION GNSS 2005 Navtech Tutorial Notes*.

[6] Skidmore, T., and Van Graas, F., "An Investigation of Tropospheric Errors on Differential GNSS Accuracy and Integrity," *Proceedings of ION GNSS 2004*: 17th International Meeting of the Satellite Division of the Institute of Navigation, 21-24 September 2004, Long Beach, CA, pp. 2752-2760.

[7] Solheim, F.S., Vivekanandan, J., Ware, R.H., and Rocken, C., "Propagation Delays Induced in GPS Signals by Dry Air, Water Vapor, Hydrometeors, and Other Particles," *Journal of Geophysical Research*, Vol. 104, No. D8, 1999, pp. 9633-9670.

[8] Champollion, C., Masson, F., Van Baelen, J. Walpersdorf, A., Chéry, J., and Doerflinger, E., "GPS Monitoring of the Tropospheric Water

Vapor Distribution and Variation During the 9 September 2002 Torrential Precipitation Episode in the Cévennes (Southern France)," *Journal of Geophysical Research*, Vol. 109, D24102, doi:10.1029/2004JD004897, 2004.
[9] Gregorius, T. and Blewitt, G., "The Effect of Weather Fronts on GPS Measurements," *GPS World*, Vol. 9, No. 5, 1998, pp. 52-60.
[10] Aonashi, K. et al., "Estimation of PWC Gradients over the Kanto Plain Using GPS Data: Validation and Possible Meteorological Implications", Earth, Planets, and Space, Vol. 52, pp. 907-912, 2000.